

Comments on tails in Schwarzschild spacetimes.

Janusz Karkowski*, Zdobysław Świerczyński⁺ and Edward Malec*

* *Institute of Physics, Jagiellonian University, 30-059 Cracow, Reymonta 4, Poland.*

⁺ *Pedagogical University, Cracow, Podchorążych 1, Poland.*

We performed a careful numerical analysis of the late tail behaviour of waves propagating in the Schwarzschild spacetime. Specifically the scalar monopole, the electromagnetic dipole and the gravitational axial quadrupole waves have been investigated. The obtained results suggest a falloff $1/t^{2l+3}$ for the general initial data and $1/t^{2l+4}$ for the initially static data.

I. INTRODUCTION

Waves propagating in a curved spacetime usually undergo backscatter; that leads to the emergence of two classes of effects, the so-called quasinormal modes (discovered by Vishveshvara [1]) and the tails. Price, who investigated the temporal behaviour of tails in 1972, has shown some kind of universality [2]. The late tail behaviour of scalar, electromagnetic and gravitational waves happened to depend only on the order of the multipole expansion. Specifically, Price argued that late tails decrease like i) $1/t^{2l+3}$ if initial data are of the type $\Psi_l = 0, \partial_t \Psi_l(r, t)|_{t=0} \neq 0$; ii) $1/t^{2l+2}$ if initial data are momentarily static, $\Psi_l \neq 0, \partial_t \Psi_l(r, t)|_{t=0} = 0$. From this one would infer that **generic tails** decay like $1/t^{2l+2}$, since a generic solution of a linear evolution equation can be superposed from two solutions specified by initial data of i) and ii). This result is usually quoted in the literature, with the notable exception of Ching et al. [3], who assign the falloff $1/t^{2l+3}$ to generic tails.

This issue has a practical significance for numerical relativity. The determination of the late tail behaviour is a nontrivial but at the same time feasible numerical task that can serve as a useful test for the accuracy and stability of numerical codes. For that reason we undertake here an attempt to clarify this ambiguous status of late tails. We study the evolution of the scalar monopole ($l = 0$), the electromagnetic dipole ($l = 1$) and the gravitational axial quadrupole ($l = 2$). The obtained results reveal a falloff $1/t^{2l+3}$ for the data $\partial_t \Psi_l \neq 0, \Psi_l = 0$, in agreement with [2], and $1/t^{2l+4}$ for the initially static initial data. The behaviour of late tails generated by initial data $\partial_t \Psi_l = 0, \Psi_l \neq 0$ differs from the relevant conclusion of [2] and, surprisingly enough, seems to be novel in the literature. Thus the general initial data have the falloff $1/t^{2l+3}$, as shown analytically by Ching et al. [3], in the examples that have been investigated.

One can predict, basing on these examples, that the l -th moment of any of the waves (scalar, electromagnetic or gravitational) will decay like $1/t^{2l+3}$ for general initial

data (in accordance with [3]) and $1/t^{2l+4}$ for the l -th moments evolving from initially static data.

II. DEFINITIONS AND EQUATIONS

The spacetime geometry is defined by the line element

$$ds^2 = -\eta_R dt^2 + \frac{dR^2}{\eta_R} + R^2 d\Omega^2, \quad (1)$$

where t is a time coordinate, R is the radial areal coordinate, $\eta_R = 1 - \frac{2m}{R}$ and $d\Omega^2 = d\theta^2 + \sin^2 \theta d\phi^2$ is the line element on the unit sphere, $0 \leq \phi < 2\pi$ and $0 \leq \theta \leq \pi$. Throughout this paper the Newtonian constant G and the velocity of light c are put equal to 1.

The propagation of the scalar, the dipole electromagnetic and the axial (quadrupole) gravitational waves is given by

$$(-\partial_t^2 + \partial_{r^*}^2)\Psi = V\Psi. \quad (2)$$

Here $r^*(R) = R + 2m \ln\left(\frac{R}{2m} - 1\right)$ is the tortoise coordinate while the potential term reads: for the $l = 0$ mode of the scalar field

$$V(R) = 2m \frac{\eta_R}{R^3}, \quad (3)$$

for the $l = 1$ (dipole) electromagnetic mode

$$V(R) = 2 \frac{\eta_R}{R^2} \quad (4)$$

and for the quadrupole axial mode of GW

$$V(R) = 6 \frac{\eta_R^2}{R^2} \left(1 - \frac{m}{R}\right). \quad (5)$$

III. NUMERICAL SCHEMES

We will choose following classes of initial data:

i) $\Psi(R, t = 0) = \sin^4\left(\pi \frac{r^* - r^*(a)}{4m}\right)$ and $\partial_t \Psi|_{t=0} = -\partial_{r^*} \Psi|_{t=0}$ for $r^* \in (r^*(a), r^*(a) + 4m)$, and $\Psi(r, 0) = \partial_t \Psi = 0$ for $r^* < r^*(a)$ or $r^* > r^*(a) + 4m$. The expected asymptotic tail falloff should be the same as for generic initial data.

ii) Symmetric initial data with $\Psi(R, t = 0) = \sin^4\left(\pi \frac{r^* - r^*(a)}{4m}\right)$ for $r^* \in (r^*(a), r^*(a) + 4m)$ and

$\Psi(r, 0) = 0$ for $r^* < r^*(a)$ or $r^* > r^*(a) + 4m$, and $\partial_t \Psi|_{t=0} = 0$ everywhere. It is shown below that the corresponding tail decays faster than that of i).

iii) $\partial_t \Psi = \sin^4\left(\pi \frac{r^* - r^*(a)}{4m}\right)$ for $r^* < r^*(a)$ or $r^* > r^*(a) + 4m$ and $\partial_t \Psi(r, 0) = 0$ for $r^* < r^*(a)$ or $r^* > r^*(a) + 4m$, while $\Psi|_{t=0} = 0$ everywhere; the tail behaviour happens to be like in i).

One finds convenient to split the wave equation (2), into the pair of first order differential equations

$$(\partial_t + \partial_{r^*})\Psi = \Phi \quad (6)$$

$$(\partial_t - \partial_{r^*})\Phi = -V(r^*)\Psi. \quad (7)$$

We use a following mesh scheme [4] (see Fig. 1)

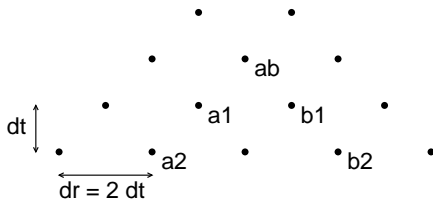


FIG. 1. This figure shows the mesh used in the numerical computations. In the one-step scheme the functions Φ_{ab} , Ψ_{ab} are computed from Eqs (9 – 11) using values at points $a1$ and $b1$. The second algorithm needs values at four points $a1$, $a2$, $b1$ and $b2$ in order to obtain Φ_{ab} , Ψ_{ab} from Eqs (14).

and two differencing schemes: the one-step implicit algorithm and the multistep Adams-like algorithm. In the first approach we approximate the equations (7) by

$$\Psi_{ab} - \Psi_{a1} = (\Phi_{ab} + \Phi_{a1}) \frac{dt}{2} \quad (8)$$

$$\Phi_{ab} - \Phi_{b1} = -(V_{ab}\Psi_{ab} + V_{b1}\Psi_{b1}) \frac{dt}{2}. \quad (9)$$

In the next step these equations are solved for Ψ_{ab} , Φ_{ab} ,

$$\Psi_{ab} = \Psi_{ab}(\Psi_{a1}, \Psi_{b1}, \Phi_{a1}, \Phi_{b1}) \quad (10)$$

$$\Phi_{ab} = \Phi_{ab}(\Psi_{a1}, \Psi_{b1}, \Phi_{a1}, \Phi_{b1}). \quad (11)$$

The second algorithm is based on the Adams-Moulton corrector formula for ordinary differential equations [4]

$$y_{n+1} = y_n + \frac{dt}{12}(5y'_{n+1} + 8y'_n - y'_{n-1}) + O(dt^4) \quad (12)$$

Applying this formula to each of the equations (7) we get approximately

$$\Psi_{ab} = \Psi_{a1} + \frac{dt}{12}(5\Phi_{ab} + 8\Phi_{a1} - \Phi_{a2}) \quad (13)$$

and

$$\Phi_{ab} = \Phi_{b1} - \frac{dt}{12}(5V_{ab}\Psi_{ab} + 8V_{b1}\Psi_{b1} - V_{b2}\Psi_{b2}) \quad (14)$$

Again this linear set of equations can be solved for Ψ_{ab} , Φ_{ab}

$$\begin{aligned} \Psi_{ab} &= \Psi_{ab}(\Psi_{a1}, \Psi_{b1}, \Psi_{a2}, \Psi_{b2}, \Phi_{a1}, \Phi_{b1}, \Phi_{a2}, \Phi_{b2}) \\ \Phi_{ab} &= \Phi_{ab}(\Psi_{a1}, \Psi_{b1}, \Psi_{a2}, \Psi_{b2}, \Phi_{a1}, \Phi_{b1}, \Phi_{a2}, \Phi_{b2}). \end{aligned} \quad (15)$$

Let us stress that these two algorithms give almost the same results, hinting at the numerical stability of our methods.

IV. NUMERICAL RESULTS

We expect the field $\Psi_l(r^*, t)$ to behave (for a fixed r^*) like

$$\lim_{t \rightarrow \infty} \Psi(r^*, t) = Ct^{-\alpha} \quad (16)$$

Our goal is to get a value of α with a reasonable accuracy. Therefore we calculate the function

$$f(t) = -\frac{d \log(\Psi_l(r^*, t))}{d \log(t)} = -t \frac{d \log(\Psi_l(r^*, t))}{dt} \quad (17)$$

which asymptotically should be equal to α .

In the first instance we analysed the case with waves, which belongs to the class i) of Sec. 3, and for the initial data of class iii) of the preceding section. The results are presented in Figs. 2 – 4 which show the temporal behaviour of the function $f(t)$ as seen at $r^* = r^*(3m) + 4\pi$. In all figures (2 – 7) below the time is put on the x-axis, which is scaled in units of m .

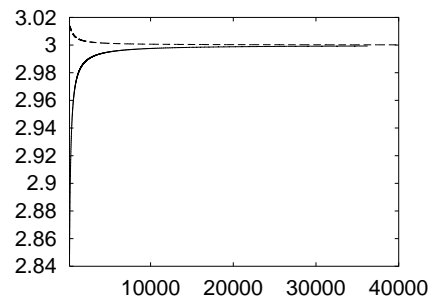


FIG. 2. The solid (general initial data) and broken line (data with $\phi = 0$), the behaviour of $f(t)$ for the scalar waves.

The numerical time ranged from 5000 m (for the gravitational and electromagnetic waves) up to 40000 m (for the scalar waves). It turned out that the precise shape of this function, without numerical noise, can be calculated using numbers with 64 significant digits (gravitational and electromagnetic cases) and the ordinary double precision numbers (scalar case). In order to achieve this aim we have used the freely distributable "qd" (quad

precision) and "arprec" (arbitrary precision) numerical libraries [5].

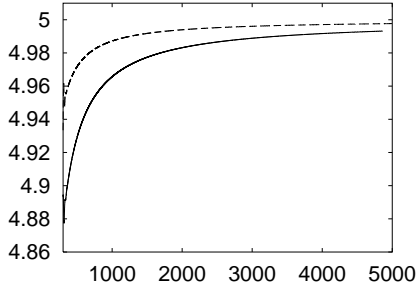


FIG. 3. The solid (general initial data) and broken line (data with $\phi = 0$), the behaviour of $f(t)$ for the electromagnetic waves.

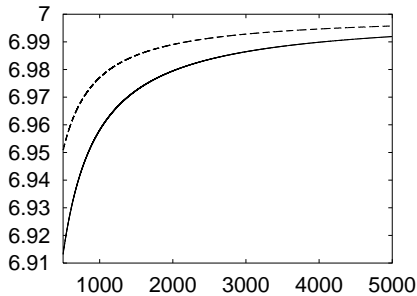


FIG. 4. The solid (general initial data) and broken line (data with $\phi = 0$), the behaviour of $f(t)$ for the gravitational waves.

The high accuracy calculations are time consuming and therefore the achieved calculational time for the scalar case exceeds by a factor of 8 the evolution time for the remaining cases. The numerically achieved values of the exponent, for the general initial data i), range from 2.999 for the scalar field, through 4.99 for the electromagnetic field up to 6.99 for the gravitational waves (figures 2 – 4, solid line). Both sets of exponents is in a good agreement with 3, 5 and 7, respectively, obtained by Ching et al. [3]. Similar results (broken line Fig. 3) have been obtained for the initial data of class iii) of the preceding section, in agreement with [2].

The momentarily static initial data (class ii) from Sec. 3) produced profiles $f(t)$ shown in Figs. 5 – 7. In this case the numerical exponents have been determined at $r^*(b) = r^*(3m) + 4\pi$ and also at another observation point, $r^* = 100m + r^*(b)$. In the first case we obtained 4, 6 and 8 (up to the fourth digit number) while in the latter case we arrived at 3.99, 5.88 and 7.84, for the scalar, electromagnetic and gravitational waves, respectively. These exponents seem to be stabilize at 4, 6 and 8 for the scalar, electromagnetic and gravitational fields, respectively; notice that the results detected at $r^* = r^*(3m) + 4\pi$ converge quicker to the prospective limiting value than those

taken at the point located farther. The asymptotic tail regime is evidently achieved quicker at a region closer to the horizon. But in both detection points, the asymptotic values of α are similar – they are very close in the case of the scalar waves, see Fig. 5 – and they differ from those suggested in [2]. The calculation of these exponents constitutes the main result of this paper.

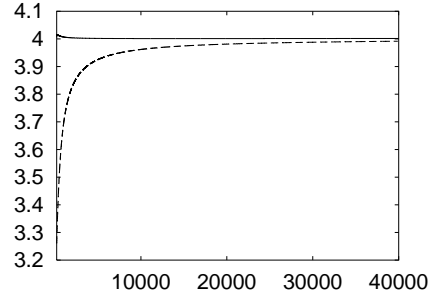


FIG. 5. Time-symmetric initial data. The solid and broken lines show the behaviour of $f(t)$ for scalar waves, as seen at the observation points $r^*(b) = r^*(3m) + 4\pi$ and $r^* = r^*(b) + 100m$, respectively.

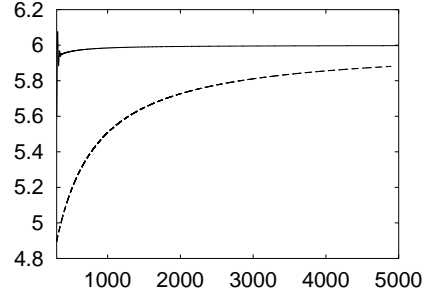


FIG. 6. Time-symmetric initial data. The solid and broken lines show the behaviour of $f(t)$ for electromagnetic waves, as seen at the observation points $r^*(b) = r^*(3m) + 4\pi$ and $r^* = r^*(b) + 100m$, respectively.

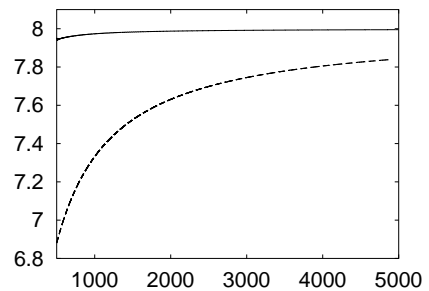


FIG. 7. Time-symmetric initial data. The solid and broken lines show the behaviour of $f(t)$ for gravitational waves, as seen at the observation points $r^*(b) = r^*(3m) + 4\pi$ and $r^* = r^*(b) + 100m$, respectively.

Acknowledgments. This work has been supported in part by the KBN grant 2 PO3B 006 23.

-
- [1] C. V. Vishveshwara, *Nature* **227**, 936(1970).
 - [2] R. Price, *Phys. Rev.* **D5**, 2419(1972).
 - [3] E. S. C. Ching P.T. Leung, W.M. Suen, K. Young, *Phys. Rev.* **D52**, 2118(1995).
 - [4] W. H. Press, S. A. Teukolsky, W. T. Vetterling and B. P. Flannery, *Numerical Recipes in C*, Oxford Press.
 - [5] Quad: Y. Hida, X. S. Li and D. H. Bailey; arprec: Y. Hida X. S. Li. H. Bailey and B. Thompson. Available at <http://users.bigpond.net.au/amiller>.